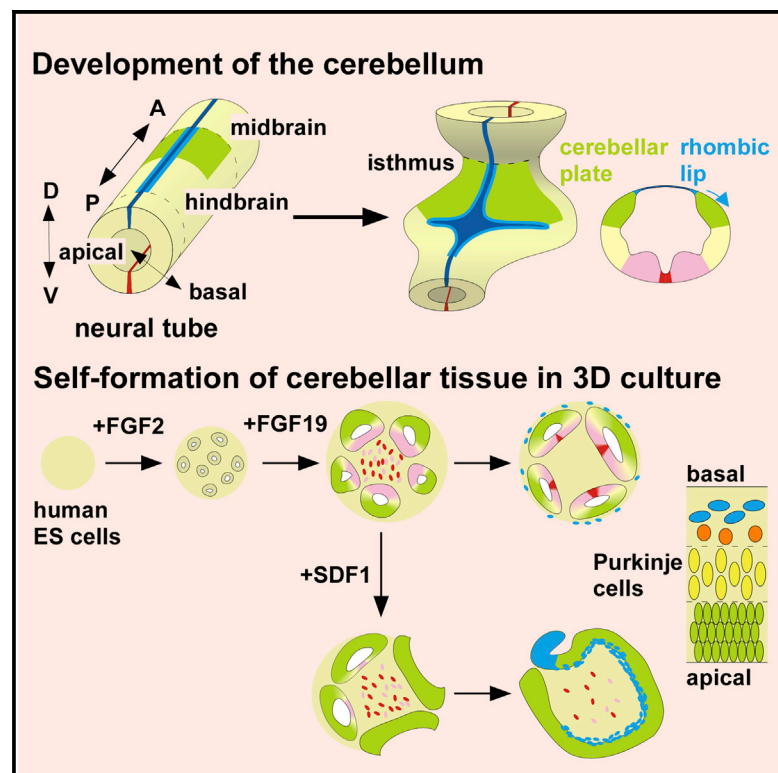# Self-Organization of Polarized Cerebellar Tissue in 3D Culture of Human Pluripotent Stem Cells

Graphical Abstract

Authors

Keiko Muguruma, Ayaka Nishiyama, ..., Kouichi Hashimoto, Yoshiki Sasai

Correspondence

muguruma@cdb.riken.jp

In Brief

Muguruma et al. developed a method to generate neurons of the cerebellum by 3D culture of human ESCs with sequential addition of growth factors. The induced cells self-organize into neural-tube-like structures with dorsoventral and apicobasal polarities. They eventually form layered structures that recapitulate cerebellar ontogenesis.

Highlights

- Neurons of the cerebellum are generated from FGF2-treated cultures of human ESCs

- The induced human Purkinje cells exhibit conserved and human-specific characteristics

- FGF19 and SDF1 promote the self-formation of polarized neural-tube-like structures

- The cerebellum is self-formed by ESC-derived cerebellar plate and rhombic lip neurons

Accession Numbers

GSE63015

CrossMark

OPEN
ACCESS
CellPress

Self-Organization of Polarized Cerebellar Tissue in 3D Culture of Human Pluripotent Stem Cells

Keiko Muguruma,[1,*] Ayaka Nishiyama,[1] Hideshi Kawakami,[2] Kouichi Hashimoto,[3] and Yoshiki Sasai[1]

[1]Laboratory for Organogenesis and Neurogenesis, RIKEN Center for Developmental Biology, Kobe 650-0047, Japan
[2]Department of Epidemiology, Research Institute for Radiation Biology and Medicine, Hiroshima University, Hiroshima, 734-8551, Japan
[3]Department of Neurophysiology, Graduate School of Biomedical and Health Sciences, Hiroshima University, Hiroshima, 734-8551, Japan
*Correspondence: muguruma@cdb.riken.jp

SUMMARY

During cerebellar development, the main portion of the cerebellar plate neuroepithelium gives birth to Purkinje cells and interneurons, whereas the rhombic lip, the germinal zone at its dorsal edge, generates granule cells and cerebellar nuclei neurons. However, it remains elusive how these components cooperate to form the intricate cerebellar structure. Here, we found that a polarized cerebellar structure self-organizes in 3D human embryonic stem cell (ESC) culture. The self-organized neuroepithelium differentiates into electrophysiologically functional Purkinje cells. The addition of fibroblast growth factor 19 (FGF19) promotes spontaneous generation of dorsoventrally polarized neural-tube-like structures at the level of the cerebellum. Furthermore, addition of SDF1 and FGF19 promotes the generation of a continuous cerebellar plate neuroepithelium with rhombic-lip-like structure at one end and a three-layer cytoarchitecture similar to the embryonic cerebellum. Thus, human-ESC-derived cerebellar progenitors exhibit substantial self-organizing potential for generating a polarized structure reminiscent of the early human cerebellum at the first trimester.

INTRODUCTION

The cerebellum is a highly ordered brain structure related to motor functions with several distinct types of cells. Its early development is conserved among amniotes. Initially, the isthmic organizer, formed at the midbrain-hindbrain boundary (MHB), induces the cerebellar plate (CP) in the dorsal region (alar plate) of rhombomere 1 (r1) (Wingate and Hatten, 1999; Joyner et al., 2000). Cerebellar cells are generated in two distinct germinal zones in r1 (Figure S1A). The ventricular zone (VZ) of the CP expresses the basic helix-loop-helix (bHLH) transcription factor Ptf1a. Ptf1a^{+} progenitors produce GABAergic neurons of the cerebellar cortex (Purkinje cells and interneurons) and of the deep cerebellar nuclei (DCN). The rhombic lip (RL) at the dorsal

margin of r1 expresses another bHLH factor, Atoh1 (also known as Math1). Atoh1^{+} progenitors generate glutamatergic neurons, including granule cells (GCs), unipolar brush cells, and large DCN projection neurons (Ben-Arie et al., 1997; Hoshino et al., 2005; Machold and Fishell, 2005; Wang et al., 2005; Fink et al., 2006). Recent knowledge on the mechanism of cerebellar differentiation has promoted technical advancement for in vitro generation of cerebellar neurons from pluripotent stem cells (Su et al., 2006; Salero and Hatten, 2007; Muguruma et al., 2010; Tao et al., 2010; Erceg et al., 2010). However, it remains unknown how the several cellular components are assembled to form the intricate structure of the cerebellum.

We previously reported that cerebellar neurons could be efficiently generated from mouse embryonic stem cells (mESCs) by recapitulating the self-inductive signaling microenvironment in 3D culture (Muguruma et al., 2010). mESCs formed isthmic organizer-like tissue in response to fibroblast growth factor 2 (FGF2) and insulin. Further inhibition of Shh signaling triggered the differentiation of the CP neuroepithelium (NE) (CPNE, hereafter) that expresses the Purkinje cell-progenitor marker Kirrel2 (also known as Neph3). On the other hand, the addition of bone morphogenetic protein (BMP) signals promoted differentiation into Atoh1^{+} GCs and Tbr1^{+} DCN neurons at the expense of Purkinje cells. Although we succeeded in induction of cerebellar neuronal components, 3D construction of cerebellar structures has not been so far recapitulated.

In the present study, we applied the self-formation principle to human ESC (hESC) culture for the generation of human cerebellar tissues in vitro. We found in vitro production of major cerebellar cell types. Of note, we demonstrated a set of electrophysiological analyses of human Purkinje cells. Moreover, we identified two factors, FGF19 and SDF1, that promote self-formation of ordered CP-like tissues in distinct manners. Here, we demonstrate that the addition of FGF19 promotes spontaneous formation of hindbrain neural-tube-like NE structures with dorsal-ventral (D-V) polarity. Sequential addition of FGF19 and SDF1 induces the generation of continuous CPNE that differentiates into a multilayered structure as seen in the cerebellar ontogenesis. NE margins form distinct RL-like germinal zones. We discuss the self-organizing nature of hESC-derived cerebellar tissues with regard to spontaneous polarity formation in 3D stem cell culture.
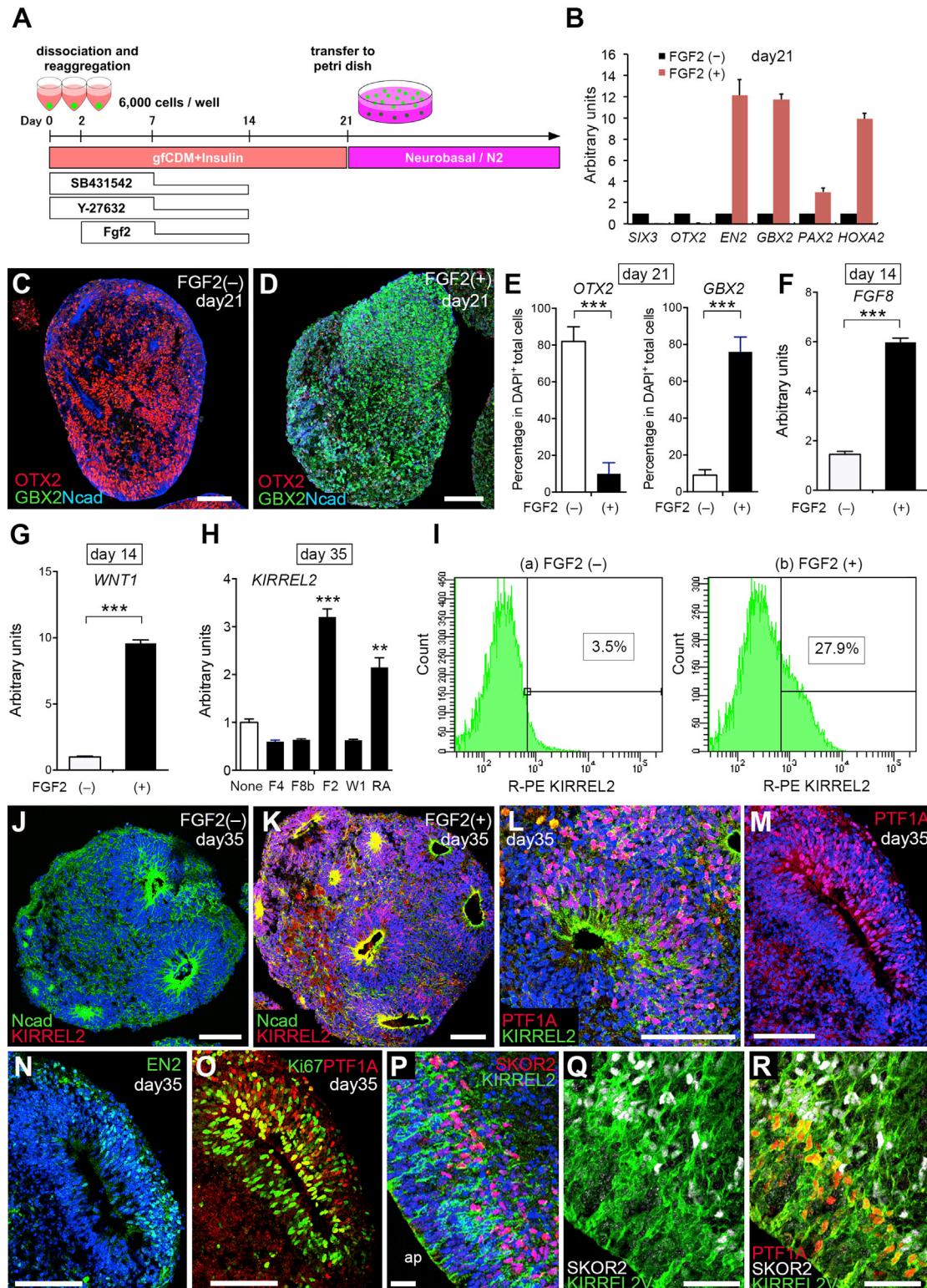
CrossMark

Figure 1. Selective Generation of Cerebellar-Plate-like NE in Self-Organizing hESC Culture

(A) Procedure for CP-specific SFEBq culture of hESCs.

(B) qPCR analysis for region-specific genes in hESC aggregate cultured for 21 days with or without FGF2.

(C and D) Immunostaining for OTX2, GBX2, and N-cadherin of hESC aggregates (day 21) cultured with or without FGF2.

RESULTS

Generation of CP in 3D hESC Culture

Our previous study revealed that mESCs robustly differentiate into cerebellar progenitors when cultured as floating aggregates in chemically defined medium supplemented with FGF2 and insulin. In contrast, hESCs only inefficiently underwent cerebellar differentiation under similar culture conditions, with or without the addition of the ROCK inhibitor Y-27632, which promotes cellular survival and reaggregation of hESCs (Watanabe et al., 2007). Here, we improved the culture conditions by using V-bottomed (not U-bottomed) 96-well plates that promote hESC reaggregation (Nakano et al., 2012) and by addition of the transforming growth factor β (TGF-ß)-receptor blocker SB431542 to inhibit mesenchymal differentiation and promote neuroectodermal differentiation (Figures S1B and S1C). Under these conditions (Figure 1A), the aggregates exhibited robust neural differentiation and expressed midbrain-hindbrain markers such as *EN2* and *GBX2*/GBX2 in an FGF2-dependent manner on days 14 and 21 (Figures 1B–1E and S1D–S1F; Table S1). Whereas FGF2 treatment suppressed the forebrain markers *SIX3* and *OTX2*/OTX2 (Figures 1B, 1D, 1E, and S1D; Table S1), it enhanced the expression of *FGF8* and *WNT1* (Figures 1F and 1G), which are implicated in the function of the isthmic organizer forming at the embryonic MHB (Thomas and Capecchi, 1990; McMahon et al., 1992; Chi et al., 2003).

KIRREL2 is among the earliest markers for the CPNE (Mizuhara et al., 2010; Figures S1A and S1G). When hESC aggregates were further cultured until day 35, a substantial population of FGF2-treated cells expressed KIRREL2 (27.9% ± 3.6% of total cells on day 35; n = 5; Figures 1H, 1I, S1H, and S1I). As seen in mESC cultures (Muguruma et al., 2010), the aggregates formed KIRREL2$^+$ hollow rosettes that resembled the NE with apical-basal polarity (Figures 1J–1R). KIRREL2$^+$ CPNE was also positive for PTF1A (mitotic CP progenitors; Figures 1L and 1M), EN2 (Figure 1N; serial section neighboring 1M), and Ki67 (Figure 1O) as seen in the embryonic CP (Mizuhara et al., 2010; Davis et al., 1988; Yamada et al., 2014; Figures S1J and S1K). We also observed accumulation of cells positive for the Purkinje cell marker SKOR2 (Figures 1P and S1L). These cells were negative for PTF1A, SOX2, and Ki67 (Figures S1M and S1N; Minaki et al., 2008) but were located just basally (peripherally) to the PTF1A$^+$ CPNE cells, indicating that they were postmitotic cells generated from the NE cells (Figures 1Q and 1R; in this triple-staining analysis, *KIRREL2*::*Venus* was used to visualize CPNE). OLIG2, another marker for early Purkinje cells and DCN precursors (Seto et al., 2014; Takebayashi et al., 2002; Figures S1G, S1K,

S1O, and S1P), was expressed in the CPNE and its periphery (Figures S1Q and S1R). OLIG2$^+$ cells did not express GSX1, a marker for early GABAergic interneuron precursors (Seto et al., 2014; Figures S1S and S1T). They did not express platelet-derived growth factor receptor α, A2B5 (early oligodendrocyte marker), or O4 (late oligodendrocyte marker), indicating that they are not oligodendrocyte precursors (data not shown).

Inhibition of ventralizing hedgehog signals by cyclopamine was required for enhanced CP specification in mESC cultures (Muguruma et al., 2010). In contrast, cyclopamine was not necessary for the differentiation of KIRREL2$^+$ cells or its enhancement in hESC cultures (e.g., 1 μM at days 7–14, 14–21, or 21–35; Figure S1U; data not shown). Together, these data show that hESC aggregates can be induced to differentiate into the CPNE in 3D culture involving transient treatments with FGF2 and insulin signals as well as the TGF-ß receptor inhibitor (FGF2-treated hESC aggregate, hereafter).

Mature Purkinje Cells from hESC-Derived CP

We next performed coculture experiments of NE progenitors with mouse external granular layer (EGL) cells derived from embryonic RL (Muguruma et al., 2010; Figure S2A), which promotes maturation of Purkinje cells. KIRREL2$^+$ CPNE cells from hESCs (sorted by fluorescence-activated cell sorting [FACS] with anti-KIRREL2 antibody; Figure S2A), not KIRREL2$^-$ cells (<0.1%), efficiently differentiated into SKOR2$^+$ cells (Figures 2A and S2B; 44.7% ± 11.2% and 35.9% ± 4.7% of HuNu$^+$ cells on coculture days 10 and 27, respectively; coculture day is shown as + div in figures), indicating that the CPNE cells have a potential to generate Purkinje cell progenitors.

We evaluated the maturation of Purkinje cells with late markers. FGF2-treated, but not FGF2-untreated, hESC cells expressed L7 (also known as PCP2, specific marker for Purkinje cells; Figures 2B, 2C, and S2C). The L7$^+$ cells also expressed other late markers calbindin (CALB1) and aldolase C and bore single long axons and multiple dendrites (Figures 2D, 2E, S2D, and S2E). L7$^+$/CALB1$^+$ cells were also positive for another marker LHX5 (Figures 2F and 2G), as seen in the embryonic CP (Morales and Hatten, 2006; Chizhikov et al., 2006). After long-term culture, LHX5$^+$/SKOR2$^+$/CALB1$^+$ Purkinje-like cells developed elaborate dendritic branches and spines that are positive for Purkinje cell-specific glutamate receptor GRID2 (GluRδ2) (Figures 2H and 2I). GRID2 was associated with CBLN1, which is expressed at the presynaptic termini of the parallel fibers (Figures 2J–2L; Uemura et al., 2010; Matsuda et al., 2010). The diameter of these hESC-derived cells was similar to that of human fetal Purkinje cells (27.2 ± 2.4 μm; referred to between 25 and

---

(E) Percentage of the OTX2- or GBX2-expressing cells in the aggregates on day 21.

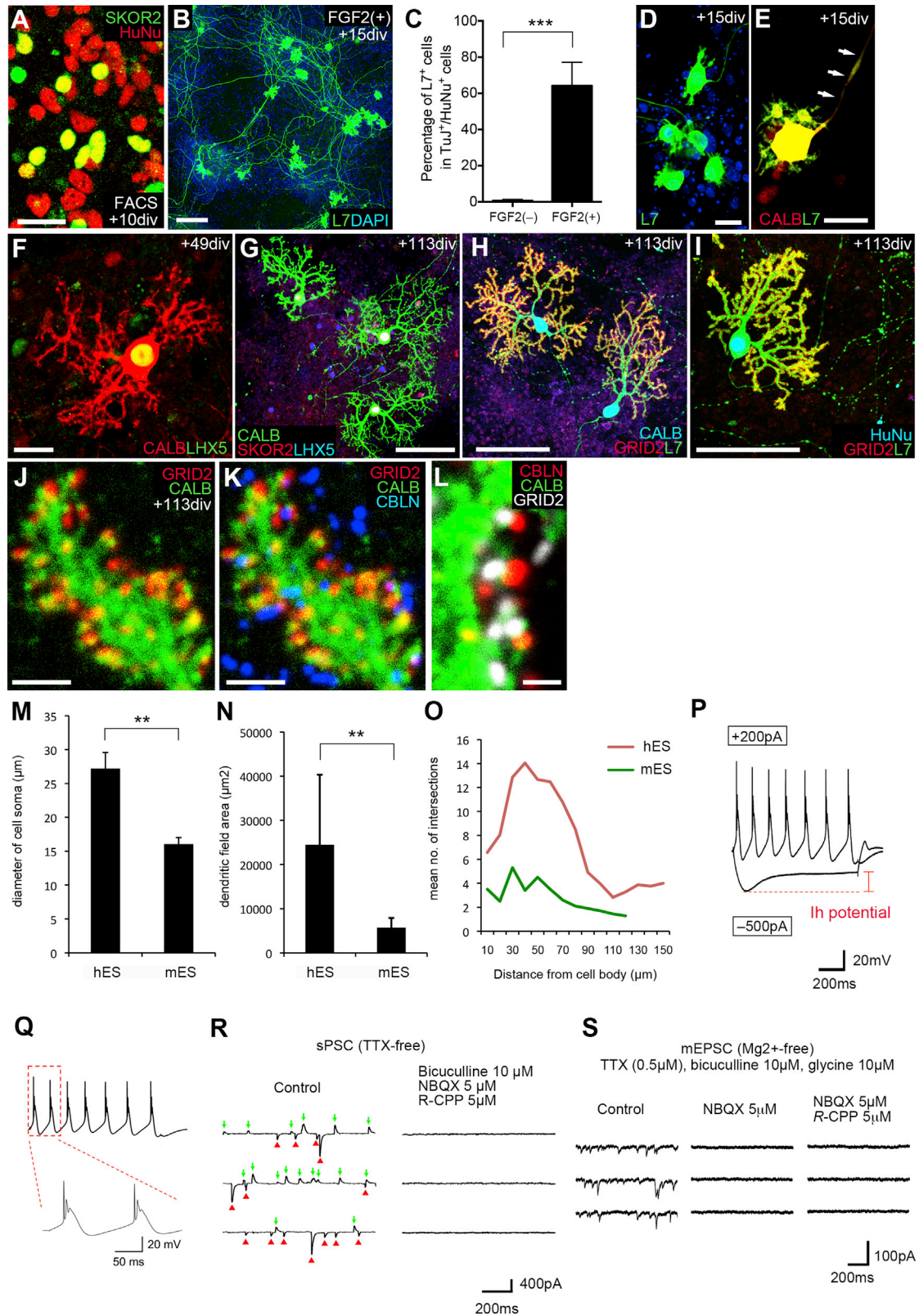(F and G) qPCR on day 14 for *FGF8* (F) and *WNT1* (G).

(H) qPCR on day 35 for *KIRREL2*. Recombinant protein (50 ng/ml in each) and retinoic acid (RA) (1 nM) was added on day 2. F2, FGF2; F4, FGF4; F8b, FGF8b; W1, WNT1.

(I) FACS analysis for the KIRREL2$^+$ cells in hESC aggregates on day 35. The percentage of the cells with fluorescence intensity larger than the threshold was shown.

(J and K) Expression of KIRREL2 and N-cadherin in the aggregates on day 35.

(L–R) Expression of cerebellar progenitor-specific markers in FGF2-treated aggregates on day 35. Immunostaining (L–P) or expression *KIRREL2*::*Venus* reporter (Q and R). ap, apical side.

The scale bars represent 100 μm (C, D, and J–O) and 25 μm (P–R). Each bar represents mean ± SD obtained from three to five independent experiments (each experiment with 24–48 aggregates). ***p < 0.001; **p < 0.01 Student's t test.

(legend on next page)

40 μm in Lapham and Markesbery, 1971). The hESC-derived cells had larger cell diameters and larger dendritic fields (Figures 2M–2O; total culture days 143–148) than mESC-derived cells (Muguruma et al., 2010; total culture days 89–97).

To examine the physiological properties of hESC-derived Purkinje cells, we performed whole-cell patch clamp recording on coculture days 108–113, when GRID2 is expressed and third-order dendrites are observed. Under the current clamp mode, hyperpolarizing and depolarizing currents were applied from the membrane potential of −60 mV in the presence of NBQX (an antagonist for AMPA-type glutamate receptor), R-CPP (an antagonist for NMDA receptor), and bicuculline (an antagonist for GABAA receptor). All hESC-derived Purkinje cells (n = 22) showed a depolarizing sag in response to hyperpolarizing current pulses (Ih potential; Figure 2P), as seen in rodents (Williams et al., 2002). Most cells (88%) elicited repetitive firing with waveform-like complex spikes to depolarizing current pulses, as seen in rodents (Figure 2Q; Gruol and Franklin, 1987; Raman and Bean, 1999). The input resistance (54.9 ± 20.4 MΩ; n = 17) was lower than that of cultured mouse cells (Hirano and Ohmori, 1986; Tabata et al., 2000). This may be because hESC-derived cells have a larger surface area than mESC-derived cells, consistent with the quantitative analysis (Figures 2M–2O). In voltage-clamp mode (−70 mV; Figure 2R), spontaneous inward (red arrowhead) and outward currents (green arrow) were observed, which were blocked by the cocktail of NBQX, R-CPP, and bicuculline, suggesting that these currents were synaptic responses generated at glutamatergic and GABAergic synapses, respectively.

Excitatory synaptic transmissions to Purkinje cells are mainly mediated by AMPA receptors (Hirano and Hagiwara, 1988; Muguruma et al., 2010). Miniature excitatory postsynaptic currents (EPSCs) that were recorded from hESC-derived cells in Mg^{2+}-free solution with TTX, bicuculline, and glycine were completely blocked by the addition of NBQX (Figure 2S; n = 5), indicating the predominant involvement of AMPA receptor.

Taken together, these results demonstrate that hESC-derived Purkinje cells have similar morphological and electrophysiological properties characteristic of bona fide neurons. In addition to Purkinje cells, two other types of neurons, neurogranin (NRGN+) Golgi cells and CALB1−/parvalbumin (PVALB+) interneurons (Figures S2F and S2G) appeared in the long-term coculture (Figures S2H–S2K).

Generation of Cerebellar GCs from hESCs

During cerebellar development, GC progenitors and DCN projection neurons arise and migrate out from the RL (Figures S1A and S3A; Altman and Bayer, 1985). It is known that BMP signals from the roof plate promote RL formation (Alder et al., 1999). We demonstrated that BMP signals are necessary for the induction of ATOH1+ RL cells from FGF2-treated mESC aggregates (Muguruma et al., 2010). In contrast, ATOH1+ cells were generated from hESCs even in the absence of BMP4 (Figure 3A). They appeared within and to the periphery of KIRREL2+ CPNE cells (Figure 3B) and expressed the RL-derivative markers BARHL1 and PAX6 as well as SOX2 (Figures 3C–3F, S3B, and S3C; Bulfone et al., 2000), as seen in the mouse CP (Figures S3A and S3D–S3F). In rodents, RL-derived cells migrate tangentially along the pial surface of the CP, forming the EGL and the nuclear transitory zone (NTZ) (giving rise to DCN neurons; Altman and Bayer, 1985; Fink et al., 2006; Figures S3A and S3D–S3J). hESC-derived cells cultured for 35 days expressed LHX2, an early postmitotic marker for NTZ (Figure S3G), in the proximity of ATOH1+/BARHL1+ cells (Figure 3G), whereas a massive accumulation of TBR1+/SMI32+ cells (characteristic of large glutamatergic projection neurons in DCN; Hoshino et al., 2005; Figure S3I) was seen in the hESC aggregate on day 53 (Figures 3H, 3I, and S3J–S3L). The addition of cyclopamine decreased ATOH1 expression (Figure S3M). Furthermore, FGF2 increased the expression of BMPs (including GDF7) on day 35 (Figure S3N) and the addition of BMP inhibitor (SB431542, dorsomorphin, and K02288) on day 14 decreased ATOH1/ATOH1 expression on day 35 (Figures S3O and S3P).

We assessed whether hESC-derived ATOH1+ cells differentiate into postmitotic mature GC neurons. Previous studies demonstrated that mESC-derived GC precursors mixed with neonatal mouse GCs exhibit robust radial axonal growth on day 5 (Figure 3J; the postnatal GCs support the maturation of the embryonic GCs; Su et al., 2006). Cells were sorted from FGF2-treated hESC aggregates on day 42 by FACS with polysialylated neural cell adhesion molecule (PSA-NCAM), which is expressed in migratory GC precursors (Figures S3Q and S3R). They were labeled with GFP and mixed with unlabeled mouse GCs to form reaggregates.

On day 5 in reaggregate culture, a number of PAX6+ cells migrated out of the reaggregates and extended radial-like fibers (TuJ1+ or MAP2+ fibers in Figures 3K and 3L). GFP+

Figure 2. Characteristics of hESC-Derived Purkinje Cells

(A and B) Immunostaining of dissociated coculture of sorted KIRREL2+ hESC-derived progenitors with mouse GCs. SKOR2+ cells appeared on coculture day 10 (B) and L7+ neurons appeared on day 15 (B).

(C) Percentage of L7+ cells. Each bar represents mean ± SD. FGF2-untreated, n = 14; FGF2-treated, n = 15; Student's t test. ***p < 0.001.

(D–L) Immunostaining of hESC-derived Purkinje cells on coculture days 15 (D and E), 49 (F), and 113 (G–L). Arrows in (E) show a CALB1+/L7+ axon. The scale bars represent 100 μm (B and G–I), 25 μm (A and D–F), 5 μm (J and K), and 1 μm (L).

(M–O) Comparison of morphology between hESC (coculture days 108–113)- and mESC (coculture days 74–82)-derived Purkinje cells. The cell soma (M) and the dendritic field (N) were larger in hESC-derived cells. Each bar represents mean ± SD. hESC-derived, n = 29 neurons; mESC-derived, n = 14; Student's t test. **p < 0.01. (O) Sholl analysis. The number of dendritic branches and dendritic length were larger in hESC-derived neurons.

(P) Voltage responses to hyperpolarizing (−500 pA) and depolarizing (+200 pA) current injections (duration; 1 s). Hyperpolarization caused Ih current (red line).

(Q) Responses to depolarizing current with magnified view.

(R) Traces of postsynaptic currents (sPSC) without (left) and with (right) bicuculline (10 μM), NBQX (5 μM), and R-CPP (5 μM). Green and red arrows indicate presumptive inhibitory and excitatory postsynaptic currents, respectively.

(S) Miniature excitatory postsynaptic currents (mEPSC) in the Mg^{2+}-free external solution with TTX (0.5 μM), glycine (10 μM), and bicuculline. Traces of control, in the presence of NBQX (5 μM) and NBQX plus R-CPP (5 μM).
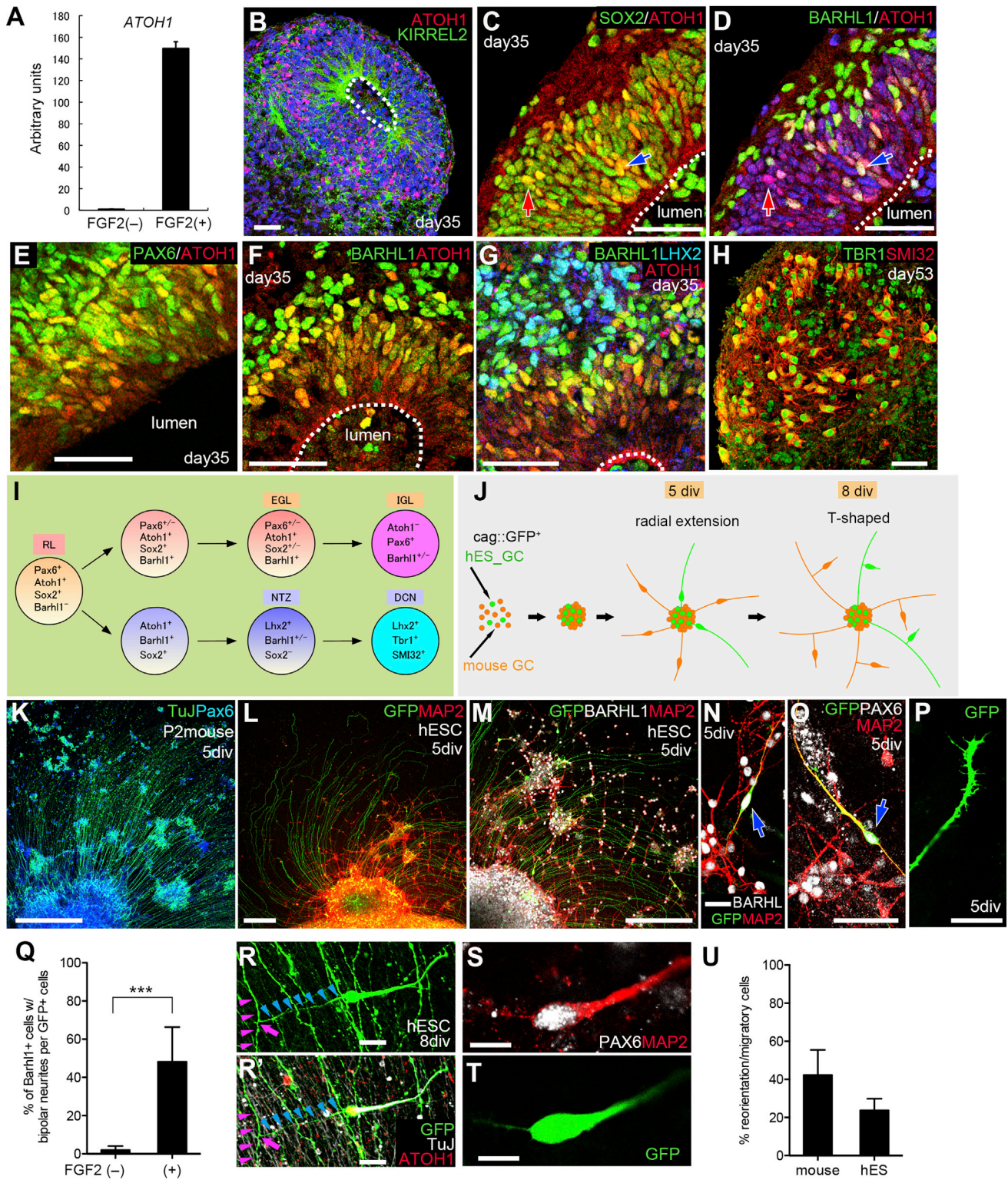
Figure 3. Generation of Granule Cells and DCN Neurons in Self-Organizing hESC Culture

(A) qPCR for *ATOH1* in hESC aggregates on day 35. Each bar represents mean ± SD obtained from three independent experiments (each experiment with 24 aggregates).

(B) Immunostaining of the aggregates on day 35. ATOH1 was expressed within and in the periphery of KIRREL2⁺ CPNE. White dots outline the lumen of the NE.

(legend continued on next page)

hESC-derived neurons extended bipolar processes (48.2% ± 18.1%) and were positive for BARHL1 and PAX6 (Figures 3M–3Q; see coexpression in vivo in Figure S3H). On day 8 in reaggregate culture, GFP+ hESC-derived neurons turned at a right angle and migrated away from the radial fibers (Figures 3R–3U), forming a T-shaped morphology that is characteristic of cerebellar GCs with parallel fibers (Su et al., 2006).

Thus, these results indicate that hESCs in 3D culture with FGF2 differentiate into a variety of cerebellar neurons including Purkinje cells, GCs, interneurons, and DCN neurons under the same culture conditions, although the efficiency of GC differentiation seems slightly low (17.6% ± 6.3% ATOH1+ cells in total cells on day 35).

FGF19 Promotes Self-Organization of Dorsoventrally Polarized Structure

Careful observation of FGF2-treated hESC aggregates on day 35 revealed two distinct types of KIRREL2+ CPNE structures, multiple small rosette-like structures (~70% cases; Figures 4A–4A''), and a few large flat-oval structures that were continuous and thicker (~30% cases; Figures 4B–4B''). Interestingly, the CPNE marker KIRREL2 was expressed on the outer side (the side facing the outer surface of the aggregate) of each flat-oval NE (Figures 4B' and 4B''), whereas it was uniformly expressed in the small rosettes (Figures 4A' and 4A''). Taking these findings together with the limited expression of KIRREL2 in the alar (dorsal) plate of the neural tube (Figure S4A), we raised a hypothesis that the flat-oval NE reflects in vivo development of the D-V axis.

To test this hypothesis, we searched for conditions that effectively promote the generation of the continuous flat-oval NE structures. Whereas BMP, WNT, and sonic hedgehog (SHH) signals (as well as their antagonists) did not show reproducible effects, FGF19 promoted the self-formation of the flat-oval NE. FGF19 is a human ortholog of mouse FGF15, which is expressed in the MHB and involved in the development of dorsal neural progenitors in the mouse and chick hindbrain (Gimeno and Martinez, 2007; Fischer et al., 2011). The addition of FGF19 (100 ng/ml) to hESC culture from day 14 prominently promoted the formation of continuous NE structures in the aggregates (Figure 4C; up to ~80%; no such effects were observed with FGF8 or FGF17; data not shown). This effect did not seem to be due to enhanced

differentiation of the CPNE in culture, because additional treatment with FGF19 did not increase the expression of KIRREL2 in FGF2-treated hESC aggregates (Figure 4D). We next examined the nature of polarity in the FGF19-treated flat-oval NE structures (Figures 4E–4H). Both KIRREL2 and PTF1A (CP markers) were expressed on the side of the flat-oval NE facing to the outside of the whole aggregate (Figure 4F). ATOH1 (marker for GC and DCN precursors) was also expressed on the outer side but in its periphery (Figure 4E). In contrast, NKX6.1 and FOXA2, specific markers for ventral neural regions (Figure S4A), were expressed on the inner side (the side facing the center of the aggregate) of the NE (Figures 4G–4I and S4B–S4D). In qPCR analysis, FGF19 substantially increased the expression of the ventral markers *FOXA2* and *SHH* and moderately increased that of *NKX6.1*, *SKOR2*, and *ATOH1* (Figure S4E). *TH*, which is expressed in dopaminergic neurons born at the ventral MHB in vivo (Ang, 2006), was also moderately increased (Figure S4F; immunostaining in Figures S4G–S4I; the increase was not as large as that induced by hedgehog signals).

The dorsal tissue differentiated on the superficial, or outer side with respect to the whole aggregate, of each of the flat-oval NE in 3D hESC culture (Figure 4J). To the periphery of KIRREL2+ CPNE, GAD65+ and LHX5+/SKOR2+ Purkinje cells were accumulated (Figures 4K–4O; day 55). These results demonstrate that FGF19 promotes the self-formation of rostral hindbrain neural-tube-like structures with a clear D-V polarity.

Self-Formation of RL-like Germinal Zones at the Margin of Stratified CP Structure

We next examined the temporal aspect of self-formation of the large flat-oval NE in FGF2+FGF19-treated hESC aggregates. On day 21, the neural tissue forming in the aggregates showed little epithelialization or apical-basal polarity (Figure 5A; no clear localization of the apical maker atypical protein kinase C [aPKC]). During days 24–28, hESC-derived NE formed with apical-basal polarity but mostly as small rosettes (Figures 5B and 5C). By day 35, the NE rosettes had transformed into large, continuous flat-oval structures with the apical side inward with respect to the oval (Figure 5D).

The finding that FGF19 has a strong influence on NE self-formation and patterning (Figure 4) prompted us to further explore

---

(C–G) Immunostaining on day 35 for GC-specific markers. (C and D) Most of Atoh1+ cells expressed SOX2. Red and blue arrows show SOX2+/ATOH1+/BARHL1− and SOX2+/ATOH1+/BARHL1+ cells, respectively. (E) A part of ATOH1+ cells expressed PAX6. (F and G) BARHL1+/ATOH1− cells lay basally to BARHL1+/ATOH1+ cells. LHX2+ cells (postmitotic cell marker in NTZ) were also located basally away from the lumen.

(H) Immunostaining on day 53 for RL-derived DCN markers (TBR1 and SMI32).

(I) Schematic of lineage-specific differentiation of RL-derived cells.

(J) Illustration of GC differentiation from hESC-derived progenitors in reaggregation culture with mouse GCs.

(K) PAX6+/TuJ1+ parallel-fiber-like bundles from reaggregated mouse cerebellar neurons (postnatal day 2).

(L and M) GFP+ hESC-derived cells radially extend their fibers and migrated from the reaggregate along the parallel fiber (PF)-like bundles on coculture day 5.
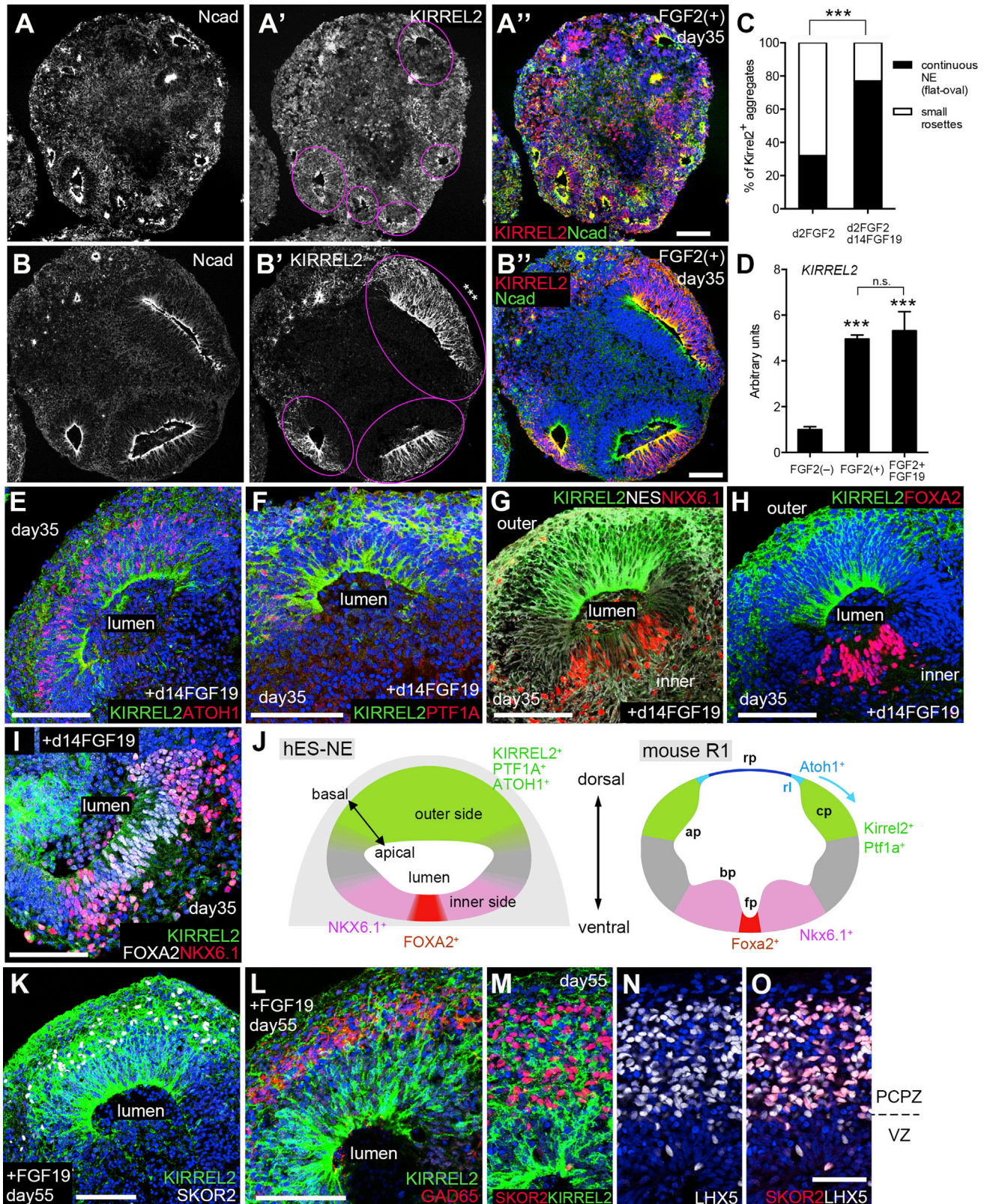
(N–P) Magnified views of migratory hESC-derived cells. The cells with MAP2+ bipolar neurites expressed BARHL1 (arrow in N) and PAX6 (arrow in O). (P) Growth cone at the tip of neurite.

(Q) Percentage of BARHL1+ cells with MAP2+ bipolar neurites in the hESCs on coculture day 5. Each bar represents mean ± SD. FGF2-untreated, n = 10; FGF2-treated, n = 12. ***p < 0.001; Student's t test.

(R–T) Characteristic T-shape morphology in GFP+ hESC-derived cells on coculture day 8. (R and R') Magenta arrowheads and arrow show the PF-like axon and the branch point, respectively. Blue arrowheads indicate the trailing process of reoriented cell. (S and T) Magnified image of a reoriented cell.

(U) Percentage of reoriented migratory cells. Each bar represents mean ± SD. mouse, mouse-derived GCs, n = 5; hES, hESC-derived neurons, n = 10.

The scale bars represent 200 μm (K–M), 50 μm (B–D, F–H, and O), and 20 μm (E, N, and P–T). EGL, external granular layer; IGL, internal granular layer; NTZ: nuclear transitory zone; RL, rhombic lip.

(legend on next page)

other signaling factors that promote 3D cerebellar development in vitro. Among several factors implicated in cerebellar development, SDF1 (also known as CXCL12; 300 ng/ml) treatment from days 28 to 35 (Figure 5E) substantially facilitated formation of a continuous NE in 3D hESC culture seemingly due to fusion of the independent ovals in each aggregate. FGF2+FGF19-treated hESCs self-form multiple flat-oval NE structures in each aggregate with dorsal-ventral polarity (as shown in Figures 4G–4I), whereas subsequent SDF1 treatment spontaneously generates continuous NE structure (shown in Figures 5F and 5G) rather than multiple flat-oval NE structures in each aggregate. The apical side is judged from the expression of KIRREL2 or aPKC, a marker for apical side of VZ. Whereas the apical side is the lumen side of the flat-oval NE structure (generated by FGF2+FGF19), it corresponds to the outer surface of the aggregate in the case of the continuous NE structure (produced by FGF2+FGF19+SDF1; Figures 5F and 5G; consistent with this idea, SOX2$^+$ VZ cells and phospho-histone H3$^+$ were on the superficial side of the NE, whereas SKOR2$^+$ Purkinje precursors were on the deep side; Figures 5H and S5A).

In the embryonic cerebellum, SDF1 is secreted from meningeal cells. Disorganization of the cerebellar structure by aberrant migration of ATOH1$^+$ GCs was reported for mice lacking SDF1 or its receptor CXCR4 (Zou et al., 1998; Zhu et al., 2002). During ontogenesis, ATOH1$^+$ and BARHL1$^+$ progenitors (expressing CXCR4; Figures S5B and S5C) migrate tangentially from the RL to form EGL, spreading under the SDF1$^+$ pial (basal) surface of KIRREL2$^+$ CPNE.

Interestingly, the addition of SDF1 to the hESC culture not only enlarged the CPNE but also promoted the differentiation of the KIRREL2$^+$ CPNE into three laminated zones along the apical-basal axis (Figures 5I–5Q and S5D–S5J; data not shown; day 35), as seen in the stratified CP during ontogenesis: from the apical to basal direction, VZ (aPKC$^+$, SOX2$^+$, and PTF1A$^+$), Purkinje cell precursor zone (LHX5$^+$, SKOR2$^+$, OLIG2$^+$, and GAD$^+$), and RL-derivative zone (ATOH1$^+$ and BARHL1$^+$). Purkinje cell precursors were found in a relatively thin layer basally adjacent to the VZ, and some of them (particularly OLIG2$^+$ early Purkinje cell precursors) coexpressed SOX2 (suggestive of mitotic progenitors). OLIG2$^+$ cells tended to be located more apically to the GAD$^+$ mature Purkinje cells (Figures S5F and S5J). BARHL1$^+$ cells were widespread in the RL-derivative zone, whereas a portion of them coexpressed ATOH1 (Figures 5N–5P and S5K–S5M). In contrast to the SDF1-treated NE, the three-layer lamination was not obvious in the SDF1-nontreated (FGF19-treated) NE, in which Purkinje

cell precursor and RL-derivative zones were not clearly separated (data not shown).

Furthermore, SDF1 induced the curled structure at the edge of continuous NE on day 35 (Figures 5G and 5R). The curled structure contained ATOH1$^+$ and BARHL1$^+$ progenitors (Figures 5S–5U) but lacked KIRREL2 expression in the tip region (Figures 5S, 5V, and 5W). ATOH1$^+$ and BARHL1$^+$ cells were also observed at a distance from the curled structure (Figures 5V and 5W), and their streams were continuous to the basal zone (RL-derivative zone) of the CP (Figures 5N–5P), reminiscent of circumferentially migrating cells on the pial (basal) surface of the CP during the ontogenesis.

In summary, FGF2+FGF19-treated hESCs can self-form continuous CP structure that recapitulates the D-V polarity of the embryonic cerebellum, whereas additional SDF1 treatment facilitates spontaneous generation of ATOH1$^+$/BARHL1$^+$ RL-like structure as well as laminated CP structures as seen at the developmental stage when cerebellar neurogenesis occurs (Figures 5X and 5Y).

DISCUSSION

Specification of Cerebellar NE in 3D hESC Culture

In this study, we have demonstrated that hESC aggregates are steered to differentiate into cerebellar progenitors when treated with FGF2 on days 2–14. Additional FGF19 and SDF1 treatments induced progenitors to self-form NE structures that mimic D-V and apicobasal arrangements of the early CP.

The inductive role of early FGF2 signals (together with insulin) for cerebellar differentiation is commonly seen in both mESC and hESC cultures (Figure 1; Muguruma et al., 2010). A major effect of FGF2 is to caudalize the NE tissue, given that it induced the caudal marker GBX2 at the cost of the rostral marker OTX2 (Figures 1B–1E). It also induced the expression of isthmic organizer factor genes *FGF8* and *WNT1* (Figures 1F and 1G). In the developing embryo, the isthmic organizer arises at the midbrain (OTX2$^+$)-hindbrain (GBX2$^+$) boundary (Wingate and Hatten, 1999; Joyner et al., 2000; Vernay et al., 2005). In our previous study using mESC culture, FGF2-induced CPNE often contained separate OTX2$^+$ and GBX2$^+$ domains within the aggregate. In our present hESC culture, FGF2-induced CPNE was predominantly GBX2-positive and expressed little OTX2. Therefore, it remains to be clarified whether the hESC-derived CPNE accompanies the formation of discrete MHB tissues or just the production of the isthmic organizer factors. Retinoic acid (RA) treatment on days 2–14 increased the expression of *KIRREL2* on day 35, but

Figure 4. FGF19 Facilitates Dorsoventral Polarization of NE in Self-Organizing hESC Culture

(A and B) Two typical structures of FGF2-induced KIRREL2$^+$/N-cadherin$^+$-NEs. (A–A'') Structure with small rosettes. (B–B'') Continuous flat-oval NE structure. Each structure was demarcated with magenta circles. Asterisks in (B') indicate the outer side of the NE with respect to the whole aggregate.

(C) Promotion of continuous flat-oval NE formation with FGF19 (100 ng/ml). ***p < 0.001 in contingency table analysis (2 × 2) with Fisher's exact test. FGF2-treated, n = 68 aggregates; FGF2+FGF19-treated, n = 83.

(D) qPCR for *KIRREL2* on day 35. Each bar represents mean ± SD obtained from three independent experiments (each experiment with 24 aggregates). ***p < 0.001 compared to FGF2-untreated. No significant difference was found between FGF2- and FGF2+FGF19-treated aggregates. Student's t test.

(E–I) Immunostaining for dorsal- or ventral-region-specific markers of FGF19-treated aggregates. (G and H) Images from adjacent sections.

(J) A scheme showing the expression pattern of dorsoventral markers in the hESC-derived NE and the mouse Rhombomere 1. ap, alar plate; bp, basal plate; cp, cerebellar plate; fp, floor plate; rl, rhombic lip; rp, roof plate.

(K–O) Immunostaining of FGF19-treated aggregates on day 55. PCPZ, Purkinje cell precursor zone; VZ, ventricular zone.

The scale bars represent 100 μm (A, B, E–I, K, and L) and 50 μm (O and apply to M and N).
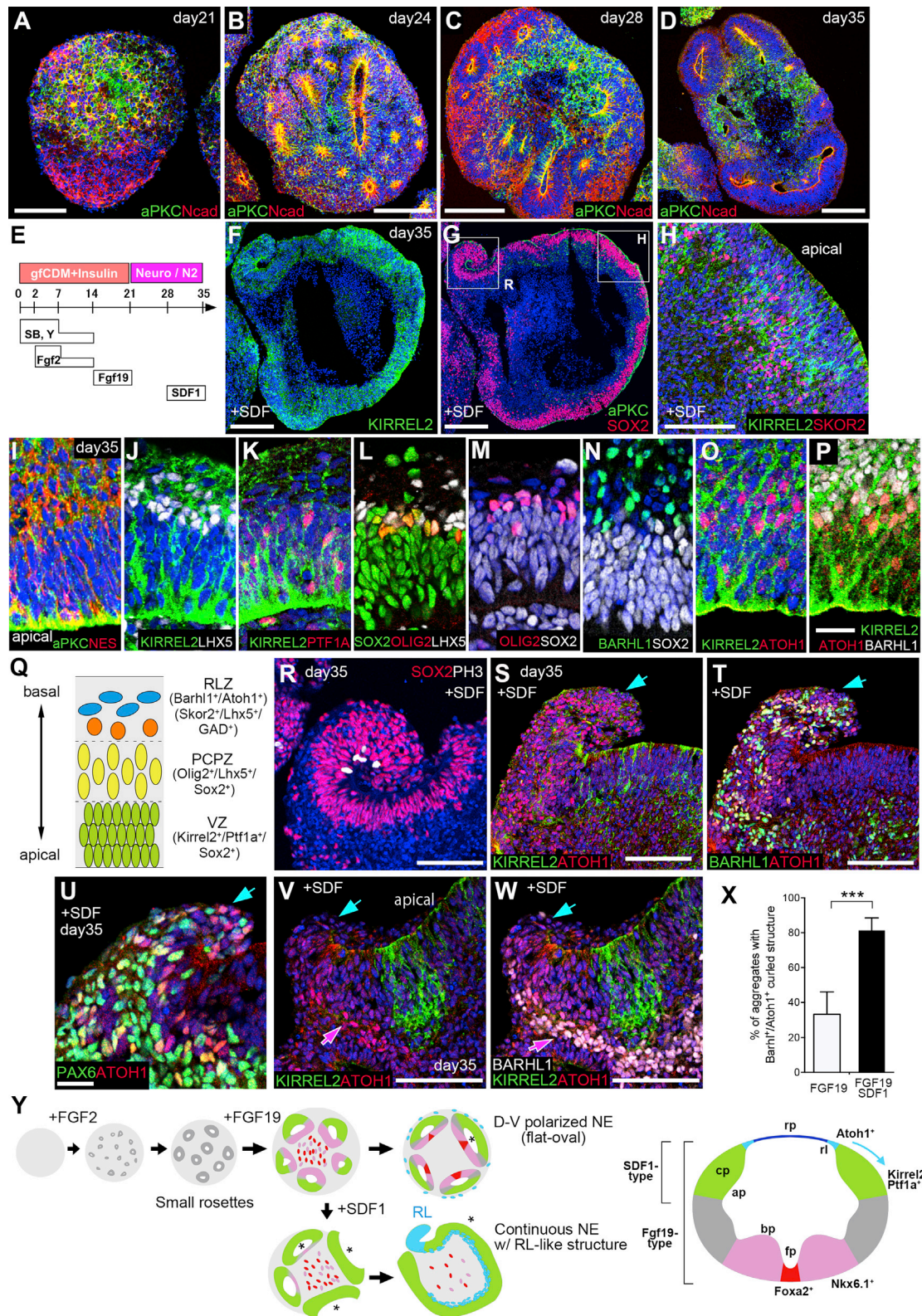
Figure 5. Self-Formation of Cerebellar NE with RL-like Structure in FGF2+FGF19+SDF1-Treated hESC Aggregate
(A–D) Self-formation of NE structure in hESC aggregate. Immunostaining for PKCζ(aPKC) and N-cadherin.
(E) Procedure of FGF2 (50 ng/ml), FGF19 (100 ng/ml), and SDF1 (300 ng/ml) treatments.

not MHB-proximity markers (*FGF8*, *WNT1*, and *EN2*) on days 14–21. Consistently, L7^{+} Purkinje cells were not observed in KIRREL2^{+} cells sorted from RA-treated hESC aggregates (data not shown). KIRREL2^{+} cells induced by RA might be the cells derived from more caudal rhombomere not r1.

KIRREL2[+] CPNE appears at day 10 in mESC culture and at day 25 in hESC culture, indicating that hESC differentiation takes ~2.5 times longer. There is another difference between the two cultures regarding the dependency on extracellular signaling. In mESC culture, efficient induction of cerebellar progenitors required additional treatment with cyclopamine. In contrast, cyclopamine treatment in hESC culture did not enhance the generation of KIRREL2^{+} cells (Figure S1U), suggesting that endogenous levels of SHH in the hESC-derived NE does not have a major role for suppressing cerebellar specification.

Generation of Human Cerebellar Neurons from hESCs

In our culture, four different cerebellar neuron precursors were generated from hESC-derived NE: Purkinje cells (L7[+] and CALB1^{+}), Golgi cells (NRGN[+], PAX2^{+}, and GAD65^{+}), GCs (ATOH1^{+}, BARHL1^{+}, and PAX6^{+}), and DCN projection neurons (LHX2^{+}, TBR1^{+}, and SMI32^{+}). Non-Golgi-type interneurons (PVALB[+], CALB1^{−}, and GAD65^{+}) were also found in the culture.

Purkinje cells are the only output neurons of the cerebellar cortex with large soma and highly arborized dendrites. hESC-derived Purkinje cells recapitulate such characteristic morphology and express Purkinje-specific GRID2 on dendrite spines, where CBLN1^{+} presynaptic GC axons terminate. They exhibit at least three electrophysiological properties of Purkinje cells known in other species: spontaneous repetitive firing (Figure 2Q; Gruol and Franklin, 1987; Raman and Bean, 1999), I$_h$ current (Figure 2P; Williams et al., 2002), and AMPA-receptor-dominant response to glutamate input (Figure 2S; Hirano and Hagiwara, 1988; Muguruma et al., 2010). We systematically demonstrate the electrophysiological properties of human Purkinje cells. In our preliminary study, we also succeeded in inducing differentiation of L7^{+} neurons from human induced pluripotent stem cells (iPSCs) (in two lines at least). Because there are several types of spinocerebellar ataxia in which Purkinje cells degenerate (e.g., SCA6), our culture may be of use for modeling those types of genetic cerebellar diseases in the future. In addition, using patient-specific iPSCs, our 3D system may be applicable to studies for understanding inborn disorders of cerebellar development, such as Dandy-Walker syndrome (Aldinger et al., 2009).

In the developing cerebellum, both GCs and DCN projection neurons are derived from the RL, which lies dorsally to the CPNE (Figures S1A and S3H). Although the addition of BMP sig-

nals was necessary for induction of RL-derived neurons in mESC culture (Muguruma et al., 2010; refer to Alder et al., 1999), it was not in the case of hESC culture (exogenous BMP4 rather showed cytotoxic effects). Because FGF2 treatment increased the expression of *BMPs* and *GDF7* (Figure S3N), enough amounts of BMP signals might be already present in the culture. Together with the fact that cyclopamine is not needed for CP induction in hESCs, these findings suggest that FGF2-induced NE from hESCs is more dorsally biased than that from mESCs.

Self-Patterning of 3D Flat-Oval NE Structures along the D-V Axis

FGF2-induced neural progenitors in the hESC aggregate initially lack clear apicobasal polarity and gradually become epithelialized during days 21–35 (Figures 5A–5D). At the beginning, the NE forms small rosettes and, particularly in the presence of FGF19, they subsequently reform into larger and thicker NE structures that eventually have flat-oval shapes. Importantly, these flat-oval NE structures are reproducibly polarized. KIRREL2^{+} and NKX6.1^{+} cells appeared in the outer and inner portions with respect to the aggregate, respectively, indicating that the alar and basal plate structures of the embryonic neural tube emerged along the superficial-deep axis of the hESC-derived NE structure (Figures 4E–4J and S4A–S4D).

In the mouse embryonic cerebellum, the FGF19 homolog FGF15 is expressed around the MHB. The addition of FGF19 to the culture increased the expression of the ventral markers *FOXA2*, *NKX6.1*, and *SHH* (Figure S4E) as well as dorsal markers such as *SKOR2* and *ATOH1* (Figure S4E). Thus, the exact effects of FGF19 on the hESC-derived NE remain to be understood, such as its direct effects on patterning, growth, and tissue architecture, as well as secondary effects.

One intriguing question regarding the self-patterning of D-V polarity in the flat-oval NE is how the superficial side reproducibly acquires its dorsal identity (cerebellar plate). One possible interpretation is that there could be some preferential accumulation of ventral-promoting signals in the central portion of the aggregates. In the aggregates with small rosettes (typical for non-FGF19-treated ones), rosette epithelia mostly consist of KIRREL2^{+} CPNE (Figure 4A) and locate in the superficial portion, whereas cells positive for ventral markers are found in the central portion of the aggregate in a dispersed manner (or as nonepithelial masses; Figure S4J), suggesting that the D-V pattern at large is regulated along the superficial-central axis in the aggregate, regardless of the presence of flat-oval NE self-formation. Another possibility is that the surface of the aggregate may have some promoting effects for dorsalization on the NE. In the embryo, such effects are considered to be conveyed by BMP signals

(F–H) Immunostaining of SDF1-treated aggregates on day 35. (F and G) These images were obtained from adjacent sections.

(I–P) Immunostaining on day 35 for cerebellar precursor-specific markers (see Figures S1 and S3).

(Q) Laminar structures found in hESC-derived cerebellar NE. RLZ, rhombic-lip-derivative zone.

(R–W) Immunostaining of curled aggregates on day 35. Cyan arrows represent RL-like structure. (S and T) and (V and W) are images of adjacent sections. Magenta arrows in (V) and (W) indicate the stream-like zone of ATOH1^{+}/BARHL1^{+} cells.

(X) Percentages of aggregates with BARHL1^{+}/ATOH1^{+} curled structure. Each bar represents mean ± SD obtained from three independent experiments. FGF19-treated: n = 38; FGF19+SDF1-treated: n = 32. ***p < 0.001; Student's t test.

(Y) Schematic of self-formation into polarized flat-oval cerebellar NE and continuous cerebellar NE with RL-like structure, depending on the combination of FGF19 and SDF1 treatments. Apical side was indicated by asterisks.

The scale bars represent 200 μm (B–D, F, and G), 100 μm (A, H–L, R–T, V, and W), and 25 μm (P and apply to I–O and U).

from the overlying epidermis (and the roof plate). Although *BMPs* were increased by FGF2 treatment (Figure S3N), the hESC aggregate in our culture does not carry these tissues on the surface. In addition, our preliminary analysis showed no substantial accumulation of pSmad1 on the superficial zone of the aggregate (data not shown).

Self-Formation of Stratified Cerebellar Tissue from CPNE and RL-like Processes

Dramatic structural changes were seen when the FGF2+FGF19-induced NE was further treated with SDF1 (Figure 5). Two major effects were (1) enhanced continuity of CPNE with lamination and (2) appearance of RL-like processes.

There are several remaining questions about these intriguing aspects of self-organization. First, how does the NE develop a large planar NE, instead of flat-oval structures, in the presence of the chemokine SDF1? Because the superficial surface of the planar NE becomes the apical side, it is likely that the NE rosettes (in which the apical side is inside) fuse to one another to form a large NE whereas their portions break, turning the inside (apical) surface out. In fact, such intermediate structures are often seen during the early phase after SDF1 treatment (Figures S5O and S5P). Second, does SDF1 treatment promote the specification into the CP? In qPCR analysis, such an effect is not obvious and the expression of the CP markers *KIRREL2* and *SKOR2* are not substantially elevated by SDF1 treatment (Figure S5N). In contrast, the ventral marker genes *NKX6.1*, *FOXA2*, and *SHH* are downregulated by SDF1, suggestive of moderate dorsalization in the hESC-derived NE. This may promote the continuity of CPNE, because ventral tissues have less chance to intervene between dorsal tissues (in the SDF1-treated aggregates, cells positive for ventral markers are dispersed in the deep portion and do not contribute to the continuous NE). Third, how does the RL process form at the edges of the planar CPNE? This question is particularly intriguing, because the hESC-derived cerebellar tissues do not include dorsal midline tissues (roof plate or TTR$^+$ choroid plexus-like tissues; Figure S5Q), which are known to promote RL formation in vivo (TTR$^+$ tissues were induced when the culture was treated with GDF7, but not without it; Figure S5R). One possibility is that the RL processes form at the break point of the NE rosettes during their reformation into a large planar NE (the NE structure in Figure S5P may support this possibility). The moderate dorsalization in the hESC-derived NE by SDF1 may also facilitate the self-formation of RL tissue, which is a dorsal structure to the KIRREL2$^+$ CPNE in vivo. Lastly, how does the CP in hESC culture self-form its three-layer lamination? The CP differentiated from the CPNE contains, in apical-basal order, the VZ, the Purkinje cell precursor zone, and the RL-derivative zone as seen in early cerebellar development. The VZ in the neural tube is generally located to the apical side. Therefore, specific questions may be how the Purkinje cell precursor zone and RL-derivative zone form at the intermediate and basal domains. In the embryo, RL derivatives migrate to form EGL in the superficial (basal) layer under the pia. In our culture, at least in the presence of SDF1, which is produced in the pia in vivo, RL derivatives form a layer on the basal side, although the culture lacks pia-like tissues. Therefore, the apical-basal order of the three zones may be caused by

certain cellular interactions across the layers, raising an interesting question for future investigation. Another open question is how much of RL derivatives in culture are generated and migrate tangentially from the RL-like processes, rather than arising vertically from the CPNE. Given the complex nature of the in vitro generation of cerebellar primordium in our culture, it will be necessary in the future to examine the generation and migration dynamics of these cells using the in toto imaging techniques with genetic marking (e.g., *ATOH1*-GFP).

In the human embryo, the cerebellar structure develops relatively slowly (O'Rahilly and Müller, 2006). The morphological appearance of the CP (thickened NE) as well as the isthmus is seen as early as at Carnegie stage (CS) 13 or 14 (postfertilization week 4), whereas the RL begins to participate in cerebellar development around CS 17 (postfertilization weeks 5 and 6). The stratification in the CP with three apical-basal layers (VZ, Purkinje cell precursor zone, and RL-derivative zone) starts at CS 18 (postfertilization week 6) and gradually proceeds. The formation of the thick EGL is first observed also around CS 23 (postfertilization week 8), when the paired cerebellar hemispheres begin to unite (resulting in the formation of vermis).

Our present study demonstrates that the early developmental events of human cerebellar primordium, occurring during these stages of the first trimester of human gestation, can be recapitulated in 3D culture of hESC aggregates, at least in part. A future challenge is to establish a long-term culture system that enables the hESC-based cerebellar self-organization culture to recapitulate the developmental events characteristic for the second trimester, for instance, the formation of intracortical and cortico-DCN neural networks and the appearance of lobular morphogenesis.

EXPERIMENTAL PROCEDURES

Cerebellar Differentiation from hESCs

hESCs were used according to the hESC research guidelines of the Japanese government. For cerebellar NE generation, hESCs were dissociated to single cells and quickly reaggregated using low-cell-adhesion 96-well culture plate with V-bottomed wells (PrimeSurface MS-9096V; Sumitomo Bakelite) in cerebellar differentiation medium (6,000 cells/well) containing growth-factor-free chemically defined medium (gfCDM) (Wataya et al., 2008), insulin (7 μg/ml), 10 μM Y-27632, and 10 μM SB431542 (Tocris Bioscience). Defining the day on which the SFEBq culture was started as day 0, recombinant human FGF2 (R&D Systems; 50 ng/ml) was added to culture on day 2. One-third dilution and full-volume replacement with gfCDM-supplemented insulin were performed on days 7 and 14, respectively.

The hESC aggregates were further subjected to long-term culture. On day 21, the floating aggregates were transferred from a 96-well plate to a 90 mm Petri dish (non-cell adhesive; Iwaki) and cultured in suspension using Neurobasal/N2 medium.

FACS

FACS analysis was performed by FACSAria II with FACSDiva software (Becton Dickinson). Primary antibody was incubated with hESC-derived cells at 4°C for 30 min. R-phycoerythrin-conjugated secondary antibodies (BD Biosciences) were used for the detection of cells labeled with primary antibodies.

Dissociated Cell Coculture for Maturation of Purkinje Cells

All animal experiments were conducted in compliance with the Guidelines for Use of Laboratory Animals of RIKEN. Cells dissociated from FGF2-treated hESC aggregates on day 35 were sorted with anti-KIRREL2 antibody. The cells

were mixed with cells derived from mouse RL tissues and cocultured as previously described (Muguruma et al., 2010).

Culture of Mixed Reaggregates

Cells from FGF2-treated hESC aggregates on day 42 were sorted with anti-PSA-NCAM antibody and labeled with GFP. Reaggregates formed by the mixture of the hESC-derived cells and neonatal mouse cerebellar cells were cultured as previously described (Su et al., 2006).

Statistical Analysis

Statistical tests were performed with the PRISM software (GraphPad, ver 6). Statistical significance was tested with Student's t test for two-group comparisons or one-way ANOVA with Tukey's post hoc test for multigroup comparison. Contingency table (2 × 2) analysis was tested with Fisher's exact test.

ACCESSION NUMBERS

The NCBI GEO accession number for RNA sequencing data reported in this paper is GSE63015 (gene-expression comparison between Fgf2-untreated and -treated hESCs).

SUPPLEMENTAL INFORMATION

Supplemental Information includes Supplemental Experimental Procedures, five figures, and three tables and can be found with this article online at http://dx.doi.org/10.1016/j.celrep.2014.12.051.

AUTHOR CONTRIBUTIONS

K.M. designed the experiments, performed most of the experiments, and wrote the manuscript. A.N. assisted with cell culture and histology. H.K. contributed to analysis with ataxia-derived cells. K.H. performed electrophysiological analysis. Y.S. designed the experiments and wrote the manuscript.

ACKNOWLEDGMENTS

REFERENCES

Alder, J., Lee, K.J., Jessell, T.M., and Hatten, M.E. (1999). Generation of cerebellar granule neurons in vivo by transplantation of BMP-treated neural progenitor cells. Nat. Neurosci. 2, 535–540.

Aldinger, K.A., Lehmann, O.J., Hudgins, L., Chizhikov, V.V., Bassuk, A.G., Ades, L.C., Krantz, I.D., Dobyns, W.B., and Millen, K.J. (2009). FOXC1 is required for normal cerebellar development and is a major contributor to chromosome 6p25.3 Dandy-Walker malformation. Nat. Genet. 41, 1037–1042.

Altman, J., and Bayer, S.A. (1985). Embryonic development of the rat cerebellum. II. Translocation and regional distribution of the deep neurons. J. Comp. Neurol. 231, 27–41.

Ang, S.L. (2006). Transcriptional control of midbrain dopaminergic neuron development. Development 133, 3499–3506.

Ben-Arie, N., Bellen, H.J., Armstrong, D.L., McCall, A.E., Gordadze, P.R., Guo, Q., Matzuk, M.M., and Zoghbi, H.Y. (1997). Math1 is essential for genesis of cerebellar granule neurons. Nature 390, 169–172.

Bulfone, A., Menguzzato, E., Broccoli, V., Marchitiello, A., Gattuso, C., Mariani, M., Consalez, G.G., Martinez, S., Ballabio, A., and Banfi, S. (2000). Barhl1, a gene belonging to a new subfamily of mammalian homeobox genes, is expressed in migrating neurons of the CNS. Hum. Mol. Genet. 9, 1443–1452.

Chi, C.L., Martinez, S., Wurst, W., and Martin, G.R. (2003). The isthmic organizer signal FGF8 is required for cell survival in the prospective midbrain and cerebellum. Development 130, 2633–2644.

Chizhikov, V.V., Lindgren, A.G., Currle, D.S., Rose, M.F., Monuki, E.S., and Millen, K.J. (2006). The roof plate regulates cerebellar cell-type specification and proliferation. Development 133, 2793–2804.

Davis, C.A., Noble-Topham, S.E., Rossant, J., and Joyner, A.L. (1988). Expression of the homeo box-containing gene En-2 delineates a specific region of the developing mouse brain. Genes Dev. 2, 361–371.

Erceg, S., Ronaghi, M., Zipancic, I., Lainez, S., Roselló, M.G., Xiong, C., Moreno-Manzano, V., Rodríguez-Jiménez, F.J., Planells, R., Alvarez-Dolado, M., et al. (2010). Efficient differentiation of human embryonic stem cells into functional cerebellar-like cells. Stem Cells Dev. 19, 1745–1756.

Fink, A.J., Englund, C., Daza, R.A.M., Pham, D., Lau, C., Nivison, M., Kowalczyk, T., and Hevner, R.F. (2006). Development of the deep cerebellar nuclei: transcription factors and cell migration from the rhombic lip. J. Neurosci. 26, 3066–3076.

Fischer, T., Faus-Kessler, T., Welzl, G., Simeone, A., Wurst, W., and Prakash, N. (2011). Fgf15-mediated control of neurogenic and proneural gene expression regulates dorsal midbrain neurogenesis. Dev. Biol. 350, 496–510.

Gimeno, L., and Martinez, S. (2007). Expression of chick Fgf19 and mouse Fgf15 orthologs is regulated in the developing brain by Fgf8 and Shh. Dev. Dyn. 236, 2285–2297.

Gruol, D.L., and Franklin, C.L. (1987). Morphological and physiological differentiation of Purkinje neurons in cultures of rat cerebellum. J. Neurosci. 7, 1271–1293.

Hirano, T., and Ohmori, H. (1986). Voltage-gated and synaptic currents in rat Purkinje cells in dissociated cell cultures. Proc. Natl. Acad. Sci. USA 83, 1945–1949.

Hirano, T., and Hagiwara, S. (1988). Synaptic transmission between rat cerebellar granule and Purkinje cells in dissociated cell culture: effects of excitatory-amino acid transmitter antagonists. Proc. Natl. Acad. Sci. USA 85, 934–938.

Hoshino, M., Nakamura, S., Mori, K., Kawauchi, T., Terao, M., Nishimura, Y.V., Fukuda, A., Fuse, T., Matsuo, N., Sone, M., et al. (2005). Ptf1a, a bHLH transcriptional gene, defines GABAergic neuronal fates in cerebellum. Neuron 47, 201–213.

Joyner, A.L., Liu, A., and Millet, S. (2000). Otx2, Gbx2 and Fgf8 interact to position and maintain a mid-hindbrain organizer. Curr. Opin. Cell Biol. 12, 736–741.

Lapham, L.W., and Markesbery, W.R. (1971). Human fetal cerebellar cortex: organization and maturation of cells in vitro. Science 173, 829–832.

Machold, R., and Fishell, G. (2005). Math1 is expressed in temporally discrete pools of cerebellar rhombic-lip neural progenitors. Neuron 48, 17–24.

Matsuda, K., Miura, E., Miyazaki, T., Kakegawa, W., Emi, K., Narumi, S., Fukazawa, Y., Ito-Ishida, A., Kondo, T., Shigemoto, R., et al. (2010). Cbln1 is a ligand for an orphan glutamate receptor δ2, a bidirectional synapse organizer. Science 328, 363–368.

McMahon, A.P., Joyner, A.L., Bradley, A., and McMahon, J.A. (1992). The midbrain-hindbrain phenotype of Wnt-1-/Wnt-1- mice results from stepwise deletion of engrailed-expressing cells by 9.5 days postcoitum. Cell 69, 581–595.

Minaki, Y., Nakatani, T., Mizuhara, E., Inoue, T., and Ono, Y. (2008). Identification of a novel transcriptional corepressor, Corl2, as a cerebellar Purkinje cell-selective marker. Gene Expr. Patterns 8, 418–423.

Mizuhara, E., Minaki, Y., Nakatani, T., Kumai, M., Inoue, T., Muguruma, K., Sasai, Y., and Ono, Y. (2010). Purkinje cells originate from cerebellar ventricular zone progenitors positive for Neph3 and E-cadherin. Dev. Biol. *338*, 202–214.

Morales, D., and Hatten, M.E. (2006). Molecular markers of neuronal progenitors in the embryonic cerebellar anlage. J. Neurosci. *26*, 12226–12236.

Muguruma, K., Nishiyama, A., Ono, Y., Miyawaki, H., Mizuhara, E., Hori, S., Kakizuka, A., Obata, K., Yanagawa, Y., Hirano, T., and Sasai, Y. (2010). Ontogeny-recapitulating generation and tissue integration of ES cell-derived Purkinje cells. Nat. Neurosci. *13*, 1171–1180.

Nakano, T., Ando, S., Takata, N., Kawada, M., Muguruma, K., Sekiguchi, K., Saito, K., Yonemura, S., Eiraku, M., and Sasai, Y. (2012). Self-formation of optic cups and storable stratified neural retina from human ESCs. Cell Stem Cell *10*, 771–785.

O'Rahilly, R., and Müller, F. (2006). The embryonic human brain: an atlas of developmental stages, Third Edition (Hoboken, NJ: Wiley-Liss).

Raman, I.M., and Bean, B.P. (1999). Ionic currents underlying spontaneous action potentials in isolated cerebellar Purkinje neurons. J. Neurosci. *19*, 1663–1674.

Salero, E., and Hatten, M.E. (2007). Differentiation of ES cells into cerebellar neurons. Proc. Natl. Acad. Sci. USA *104*, 2997–3002.

Seto, Y., Nakatani, T., Masuyama, N., Taya, S., Kumai, M., Minaki, Y., Hamaguchi, A., Inoue, Y.U., Inoue, T., Miyashita, S., et al. (2014). Temporal identity transition from Purkinje cell progenitors to GABAergic interneuron progenitors in the cerebellum. Nat. Commun. *5*, 3337.

Su, H.-L., Muguruma, K., Matsuo-Takasaki, M., Kengaku, M., Watanabe, K., and Sasai, Y. (2006). Generation of cerebellar neuron precursors from embryonic stem cells. Dev. Biol. *290*, 287–296.

Tabata, T., Sawada, S., Araki, K., Bono, Y., Furuya, S., and Kano, M. (2000). A reliable method for culture of dissociated mouse cerebellar cells enriched for Purkinje neurons. J. Neurosci. Methods *104*, 45–53.

Takebayashi, H., Ohtsuki, T., Uchida, T., Kawamoto, S., Okubo, K., Ikenaka, K., Takeichi, M., Chisaka, O., and Nabeshima, Y. (2002). Non-overlapping expression of Olig3 and Olig2 in the embryonic neural tube. Mech. Dev. *113*, 169–174.

Tao, O., Shimazaki, T., Okada, Y., Naka, H., Kohda, K., Yuzaki, M., Mizusawa, H., and Okano, H. (2010). Efficient generation of mature cerebellar Purkinje cells from mouse embryonic stem cells. J. Neurosci. Res. *88*, 234–247.

Thomas, K.R., and Capecchi, M.R. (1990). Targeted disruption of the murine *int-1* proto-oncogene resulting in severe abnormalities in midbrain and cerebellar development. Nature *346*, 847–850.

Uemura, T., Lee, S.-J., Yasumura, M., Takeuchi, T., Yoshida, T., Ra, M., Taguchi, R., Sakimura, K., and Mishina, M. (2010). Trans-synaptic interaction of GluRdelta2 and Neurexin through Cbln1 mediates synapse formation in the cerebellum. Cell *141*, 1068–1079.

Vernay, B., Koch, M., Vaccarino, F., Briscoe, J., Simeone, A., Kageyama, R., and Ang, S.L. (2005). Otx2 regulates subtype specification and neurogenesis in the midbrain. J. Neurosci. *25*, 4856–4867.

Wang, V.Y., Rose, M.F., and Zoghbi, H.Y. (2005). *Math1* expression redefines the rhombic lip derivatives and reveals novel lineages within the brainstem and cerebellum. Neuron *48*, 31–43.

Watanabe, K., Ueno, M., Kamiya, D., Nishiyama, A., Matsumura, M., Wataya, T., Takahashi, J.B., Nishikawa, S., Nishikawa, S., Muguruma, K., and Sasai, Y. (2007). A ROCK inhibitor permits survival of dissociated human embryonic stem cells. Nat. Biotechnol. *25*, 681–686.

Wataya, T., Ando, S., Muguruma, K., Ikeda, H., Watanabe, K., Eiraku, M., Kawada, M., Takahashi, J., Hashimoto, N., and Sasai, Y. (2008). Minimization of exogenous signals in ES cell culture induces rostral hypothalamic differentiation. Proc. Natl. Acad. Sci. USA *105*, 11796–11801.

Williams, S.R., Christensen, S.R., Stuart, G.J., and Häusser, M. (2002). Membrane potential bistability is controlled by the hyperpolarization-activated current $I(H)$ in rat cerebellar Purkinje neurons *in vitro*. J. Physiol. *539*, 469–483.

Wingate, R.J.T., and Hatten, M.E. (1999). The role of the rhombic lip in avian cerebellum development. Development *126*, 4395–4404.

Yamada, M., Seto, Y., Taya, S., Owa, T., Inoue, Y.U., Inoue, T., Kawaguchi, Y., Nabeshima, Y., and Hoshino, M. (2014). Specification of spatial identities of cerebellar neuron progenitors by ptf1a and atoh1 for proper production of GABAergic and glutamatergic neurons. J. Neurosci. *34*, 4786–4800.

Zhu, Y., Yu, T., Zhang, X.-C., Nagasawa, T., Wu, J.Y., and Rao, Y. (2002). Role of the chemokine SDF-1 as the meningeal attractant for embryonic cerebellar neurons. Nat. Neurosci. *5*, 719–720.

Zou, Y.-R., Kottmann, A.H., Kuroda, M., Taniuchi, I., and Littman, D.R. (1998). Function of the chemokine receptor CXCR4 in haematopoiesis and in cerebellar development. Nature *393*, 595–599.